Climate Dynamics (2001) 17:187–203

F. Codron

Sensitivity of the tropical Pacific to a change of orbital forcing in two versions of a coupled GCM

Received: 14 December 1999 / Accepted: 24 May 2000

Abstract The changes of the variability of the tropical Pacific ocean forced by a shift of six months in the date of the perihelion are studied using a coupled tropical Pacific ocean/global atmosphere GCM. The sensitivity experiments are conducted with two versions of the atmospheric model, varied by two parametrization changes. The first one concerns the interpolation scheme between the atmosphere and ocean models grids near the coasts, the second one the advection of water vapor in the presence of downstream negative temperature gradients, as encountered in the vicinity of mountains. In the tropical Pacific region, the parametrization differences only have a significant direct effect near the coasts; but coupled feedbacks lead to a 1 °C warming of the equatorial cold tongue in the modified (version 2) model, and a widening of the western Pacific large-scale convergence area. The sensitivity of the seasonal cycle of equatorial SST is very different between the two experiments. In both cases, the response to the solar flux forcing is strongly modified by coupled interactions between the SST, wind stress response and ocean dynamics. In the first version, the main feedback is due to anomalous upwelling and leads to westward propagation of SST anomalies; whereas the version 2 model is dominated by an eastward-propagating thermocline mode. The main reason diagnosed for these different behaviors is the atmospheric response to SST anomalies. In the warmer climate simulated by the second version, the wind stress response in the western Pacific is enhanced, and the off-equatorial curl is reduced, both effects favoring eastward propagation through thermocline depth anomalies. The modifications of the simulated seasonal cycle in version 2 lead to a change in ENSO behavior. In the control climate, the interannual variability in the eastern Pacific is dominated by warm events, whereas cold events tend to be the more extreme ones with a shifted perihelion.

F. Codron
Laboratoire de Météorologie Dynamique du CNRS, Paris, France
E-mail: Codron@atmos.washington.edu

1 Introduction

Although the top-of-atmosphere incident solar forcing (ISF) at the equator has an essentially semi-annual period, the central and eastern equatorial Pacific sea surface temperature evolution is dominated by an annual cycle. The forcing of the ocean temperature must thus have an annual component, although it need not be very strong: as reminded by Schneider (1996), the heat storage in the oceanic mixed layer tends to relatively enhance the SST response to lower frequency harmonics of the forcing.

A possible explanation lies in the north-south asymmetry of the mean climate state, the position of the ITCZ to the north forcing mean southerly trades on to the equator. The symmetric solar forcing can then yield an antisymmetric response in equatorial upwelling and vertical mixing, as shown by Li and Philander (1996) using a simple model. This response can be further amplified by various feedbacks, involving e.g., the meridional wind stress or the stratus clouds (Philander et al. 1996). Since the shallow oceanic mixed layer of the eastern equatorial Pacific makes the surface temperature very sensitive to the influence of vertical mixing (Chen et al. 1994; Koberle and Philander 1994; Chang 1993, 1996), the annual response can become dominant. The SST anomalies also display westward propagation into the central Pacific, which seems due to coupled feedbacks between the SST and zonal wind stress (Nigam and Chao 1996; Xie 1994).

The ISF at the equator also has a weak annual cycle due to the eccentricity of the Earth's orbit, the perihelion being presently in January. To test the sensitivity of the seasonal cycle and the associated coupled mechanisms to this annual component, a coupled atmosphere-Pacific Ocean GCM was forced by a change of six months of the date of the perihelion. The ISF is thus increased in the Northern Hemisphere summer, and decreased in winter, with a maximum difference in the summer hemisphere. These conditions are similar, although not

identical, to those of 10 000 years ago during the early Holocene: the tilt of the Earth's axis was different, and the extent of the ice sheets over the Northern Hemisphere continents was much larger than today. The use of a limited area ocean GCM, and the short length of the simulations, also prevent any adjustment of the global oceanic circulation in the model. These simulations should thus be considered more as sensitivity experiments rather than attempts to simulate the Holocene climate. It can however by reasonably expected that the main change between the early Holocene and today near the equator is the perihelion date, so the comparison of our results with paleo-climate data is to some extent justified.

The main climatic impact found in data and previous modeling studies of the Holocene climate (Masson and Joussaume 1997; de Noblet et al. 1996; Hewitt and Mitchell 1996, 1998; Hall and Valdes 1997; Vettoretti et al. 1998; Kutzbach and Gallimore 1988) is a warming of the Northern Hemisphere continents in summer, and an intensification of the African and Asian monsoons. For the tropical Pacific, Bush (1999) found an enhanced seasonal cycle, caused by stronger summer trade winds linked to the stronger monsoon. He used an increased obliquity and only a 3-month perihelion shift, but Giese and Carton (1994) found a similar result in a low-resolution model with only a 6-month perihelion change. On the other hand, DeWitt and Schneider (1998) found only a 1–2 month delay of the eastern Pacific seasonal cycle. The mixed layer temperature sensitivity was attributed both to the surface heat fluxes, and to upwelling and zonal advection changes forced by the zonal wind stress differences.

This experiment also provides a good way to explore the interactions between the seasonal cycle and ENSO-related variability. As there is no interannual forcing nor model change, any difference in the characteristics of ENSO must come from the modified seasonal cycle or mean climate state. Data evidence for past climates suggest that extreme El Niño events were absent during the early Holocene, and that strong events appeared only during the late Holocene (−6000 years) (Sandweiss et al. 1996; DeVries et al. 1997; McGlone et al. 1992; Rodbell et al. 1999). No model has yet been able to reproduce this ENSO modification. DeWitt and Schneider (1998) found a shift in the preferred seasonal phase following the eastern Pacific seasonal cycle change, but no amplitude difference. Otto-Bliesner (1999) also found no change of ENSO characteristics for a middle Holocene simulation, but the correlation of ENSO with Sahel precipitation was lowered considerably, suggesting that other indirect evidence of past ENSO activity could be not fully reliable.

The simulation with a shifted perihelion and comparison with the control climate was repeated with two versions of the IPSL coupled tropical Pacific GCM. The second and most recent version includes two parametrization changes intended to improve the simulation of the eastern Pacific region. They have little direct impact far from the coast, but lead to a warming of the whole equatorial Pacific through coupled feedbacks. The mechanisms of the response of the seasonal cycle were surprisingly different in the two versions, so both are analyzed here to show the impact of the basic state changes on the sensitivity of the model. A quick description of the coupled model and the two versions differences, and of the simulated climate, is given in Sect. 2. Section 3 examines the influence of orbital forcing on the equatorial Pacific seasonal cycle, and the discusses the differences between the two versions; Sect. 4 focuses on interannual variability modifications. The main results are then summed up in Sect. 5.

2 Model description and control climate

2.1 The coupled model

The atmospheric component of the ISPL tropical coupled model is version 5b of the LMD grid-point GCM, close to the one described by Harzallah and Sadourny (1995). Its main features are summarized in Table 1. The horizontal resolution is 64×50 points equally spaced in longitude and sine of latitude, which provides a better meridional resolution in the tropics. The vertical structure involves 11 layers.

The oceanic model is the GCM developed at LODYC (Andrich et al. 1988). The domain covers the tropical Pacific between 47°S and 50°N. The limited area makes it easier to obtain a realistic control climate without too much flux correction in the domain of interest, and allows a quicker spin-up of the model and a higher resolution. The horizontal resolution is 0.75° in longitude, in the meridional direction it extends from 0.33° near the equator to 1.5° at the boundaries. In the ocean interior, temperature and salinity are restored towards climatological values (Levitus 1982) to account for the heat and salt fluxes through the meridional boundaries. The restoring coefficient decreases to 0 at the equator and at the coasts. On the vertical it increases from 0 at the surface to 13 days^{-1} at 150 m, then decreases to 2 years^{-1} at the bottom.

The two models are coupled using the delocalized physics method developed by Vintzileos and Sadourny (1997) in which the physical parametrizations of the atmospheric model are computed on vertical columns constructed over the ocean model grid, thus allowing a better representation of non-linearities in the influence of surface conditions on the atmosphere. The information exchange takes place every hour, i.e., every ocean model time step.

Climatological SSTs (Reynolds and Marsico 1993) are prescribed over oceanic areas not covered by the model. To avoid discontinuities at the meridional boundaries of the ocean model, the heat flux received by the ocean is corrected outside of the 20°S–20°N band, reaching 40 $\text{W} \cdot \text{m}^{-2} \cdot \text{K}^{-1}$ at the boundaries. The

Table 1 LMD AGCM characteristics

Horizontal resolution	64 longitude × 50 sine of latitude
Horizontal advection	Upstream scheme
Dynamio equations	Sadourny (1975)
Lateral diffusion	Bi-Laplacian
Vertical coordinate	11 layers in $\sigma = p/p_s$
Thermodynamic variable	Potential enthalpy $H = C_p T \cdot (p_s/p)^{\kappa}$
Shortwave radiation	Fouquart and Bonnel (1980)
Longwave radiation	Mororette (1991)
Clouds parametrization	Le Treut and Li (1991)
Boundary layer	Bulk aerodynamic
Convection schemes	Manabe and Strickler (1964) saturated case Kuo(1965) unsaturated case

simulations start with an ocean at rest with climatological temperature and salinity. The atmosphere is initialized from a previous run on 1st January, 1986. The first year of each simulation is removed before analysis to account for the coupled model adjustment.

2.2 Changes in the parametrizations

The basic version (version 1) of the coupled model was used by Vintzileos et al. (1999a, b). Later, two parametrization changes were introduced in the atmospheric model. The first one is a modification of the scheme for the interpolation of atmospheric variables onto the ocean model grid, a component of the delocalized physics coupling method. The scheme has been improved for a better representation of ocean/land contrasts near the coasts, as described in Codron et al. (2000a). The interpolation scheme remained identical in the ocean interior.

The most important modification concerns the horizontal water vapor advection scheme: a limitation of the advected water vapor has been added, based on the saturation mixing ratio. This prevents spurious advection from warm to cool areas, and leads to a better simulation of the humidity and precipitation distribution near mountain regions. Again, this modification has little impact over the open ocean, but the changes in the rainfall over the Andes have a strong influence on the wind stress over the far eastern Pacific.

The two simulations using version 1 last 30 years each, they will be designed Ctl1 for the control run, and Per1 for the run with a six month shift of the perihelion. The version 2 with the two added atmospheric parametrization was used for two more experiments of also 30 years each, called Ctl2 and Per2.

2.3 Mean control climate

The mean climate and seasonal and interannual variability of the Ctl1 simulation are detailed in Vintzileos et al. (1999a, b). The differences between Ctl1 and Ctl2 simulations are the subject of another paper (Codron et al. 2000b), and are only briefly presented here.

Figure 1 shows the mean tropical Pacific SST simulated in runs Ctl1 and Ctl2, together with the Reynolds and Marsico (1993) observations. Both simulations are not too far from the observed climate. In Ctl1, the main deficiency is an extension of the equatorial cold tongue too far to the west, and an erosion of the western Pacific warm pool. In the east, the SST is too warm at the coast. The cooler area near 5°S, 85°W is due to spurious winter upwelling, and is thus not realistic. The improvement of the Andes rainfall in Ctl2 leads to the correction of this default in Ctl2. The subsequent warming then propagates westwards with a maximum at the equator. The extent of the warm pool and penetration of the cold tongue are thus better represented in Ctl2, however the south-eastern part of the basin is too warm. This may be attributed in part to the lack of simulated stratus clouds.

The effect of the modified advection scheme is clear in Fig. 2, which shows the mean precipitation and surface wind stress for runs Ctl1 and Ctl2, as well as for observed data: MSU (Spencer 1993) precipitation and FSU (Stricherz et al. 1992, 1997) pseudo wind stress. The spurious heavy rainfall over the summits of the Andes and New Guinea observed in Ctl1 have disappeared in Ctl2. Over the ocean, the cool equator and strong meridional SST gradient in Ctl1 lead to a strong and narrow ITCZ centered at 6–8°N. The SPCZ is on the other hand very weak. In Ctl2, the warm pool covers a larger area, and there is a widening of the ITCZ towards the equator, and a strengthening of the SPCZ.

The wind stress is consistent with the precipitation patterns: in Ctl1 strong easterly trades cover the whole basin, while in Ctl2 the wind speed decreases over the western Pacific convective areas.

The seasonal cycle of the equatorial Pacific SST for the two control runs and the Reynolds and Marsico (1993) observations is shown in Fig. 3. In all the article, equatorial will mean a 2°S–2°N average. The phase and westward propagation of the eastern

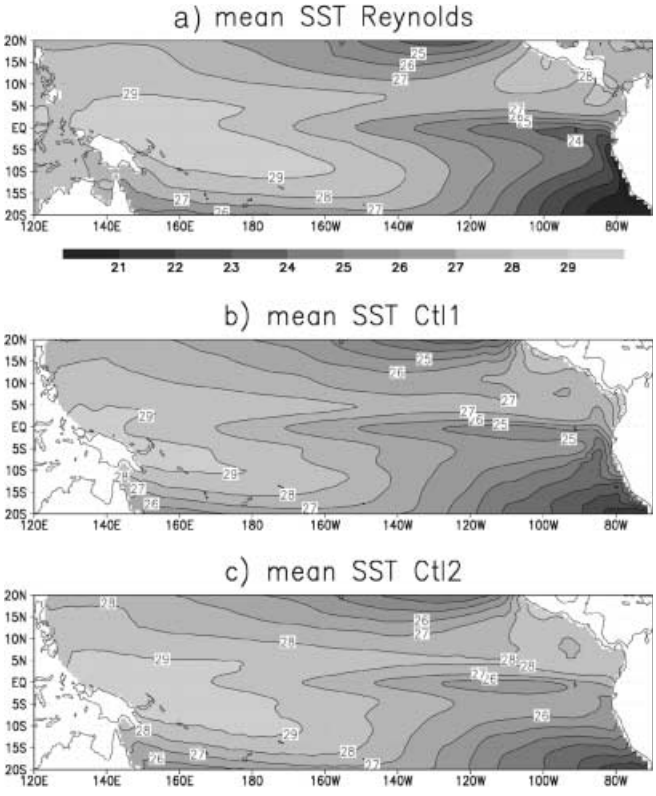

Fig. 1a–c Mean sea surface temperature for **a** Reynolds 1981–98 SST and runs, **b** Ctl1, and **c** Ctl2

Pacific SST seasonal cycle in Ctl1 is similar to the observed one, but the amplitude is much too low. The main problem is the presence of strong anomalies near the coast between 80 and 90°W, which propagate into the ocean interior. These discrepancies are removed in Ctl2, and the simulated seasonal cycle is now much closer to the observations.

3 Seasonal cycle sensitivity

The main changes in the global climate induced by the shift in perihelion date in both versions are similar to previous simulations: during the northern hemisphere summer, the African and Asian monsoons are strengthened and shifted northward. The 200hPa velocity potential (not shown) indicates an increase of the upper level divergence over these regions, while the convergence increases over the central Pacific. The situation is reversed in winter, when the main precipitation areas move over the Indian and west Pacific oceans, which cool less than the neighbouring African and Australian land masses. We now focus on the equatorial Pacific changes.

3.1 Version 1 sensitivity

The equatorial SST seasonal cycle of the Per1 simulation, and the difference with the Ctl1 run, are shown on Fig. 4. The eastern Pacific seasonal cycle has weakened

considerably, and is now almost semi-annual. However, the discrepancies at the coast are still present, and have a more annual influence. The westward propagation has completely disappeared. Indeed, the Per1-Ctl1 SST difference displays westward propagation in the central Pacific of similar amplitude as the Ctl1 seasonal cycle, but of opposite phase. As a result, the central and western Pacific have in Per1 a weak annual cycle, with a cold phase in spring and warm phase in autumn.

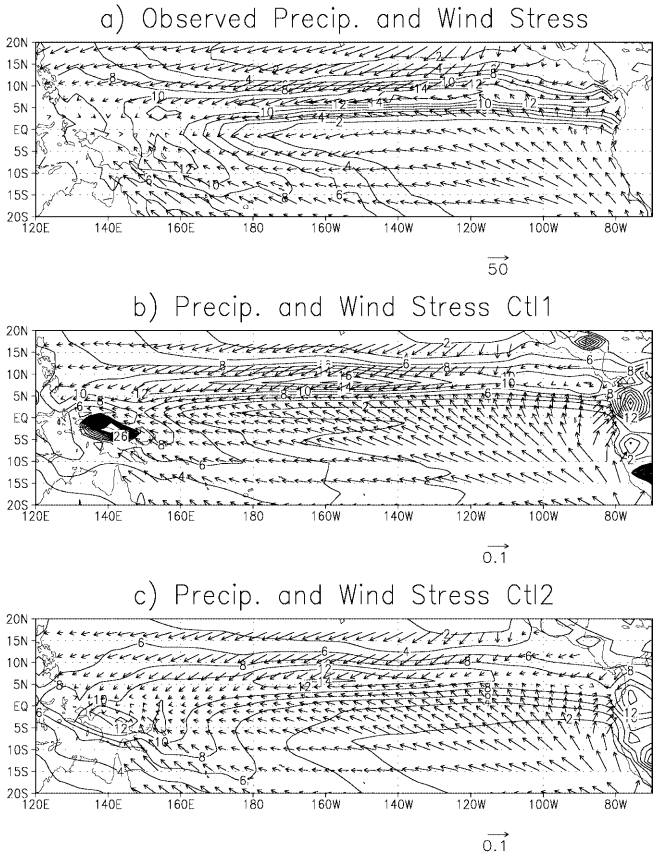

Fig. 2 **a** Mean precipitation (*contour*) and wind stress (*arrows*) for MSU and FSU observations **b** runs Ctl1, and **c** Ctl2. Precipitation is in mm/day, and the wind stress is in $m \cdot s^{-1}$ for the model and in $m^2 \cdot s^{-2}$ for the FSU data

The differences in the surface heat flux into the ocean (Fig. 5) follow the shortwave flux driven by the ISF, with a maximum in summer and a minimum in winter. The amplitude is stronger in the west, because of the cloud albedo negative feedback on SST, more efficient in warm SSTs regions (Ramanathan and Collins 1991). In July–August, the cooler SST in Per1 near the dateline, and the enhanced large-scale subsidence forced by the monsoon, decrease the cloud amount at the equator and further increase the solar forcing. The situation is exactly reversed in winter, more cloudiness in Per1 blocking the shortwave radiation, which is already reduced. In the extreme west, the SST differences are more in phase with the heat flux ones, leading to reduced forcing. The shortwave flux thus provides a negative feedback on SST differences in the western Pacific, but does not explain the westward propagation.

The answer may be found in the zonal wind stress differences (Fig. 5), which are located to the west of SST anomalies and follow their westward migration. The effect of the zonal wind on SST through anomalous upwelling and entrainment is a classical candidate for the westward propagation of eastern Pacific SST seasonal anomalies (Nigam and Chao 1996). The anomalous westerlies in summer in the east contradict the results of other simulations (Giese and Carton 1994; Bush 1999). In our model, the oceanic warming is maximum at the equator in the eastern Pacific because the mixed layer is shallower, and the ITCZ to the north reflects more incoming solar radiation. There is thus no northward movement of the ITCZ, and no increased northward trades.

Depth-longitude sections of the temperature at the equator (Fig. 6) give another picture of the seasonal differences. The surface anomalies extend over all the mixed layer depth and clearly propagate westward. In

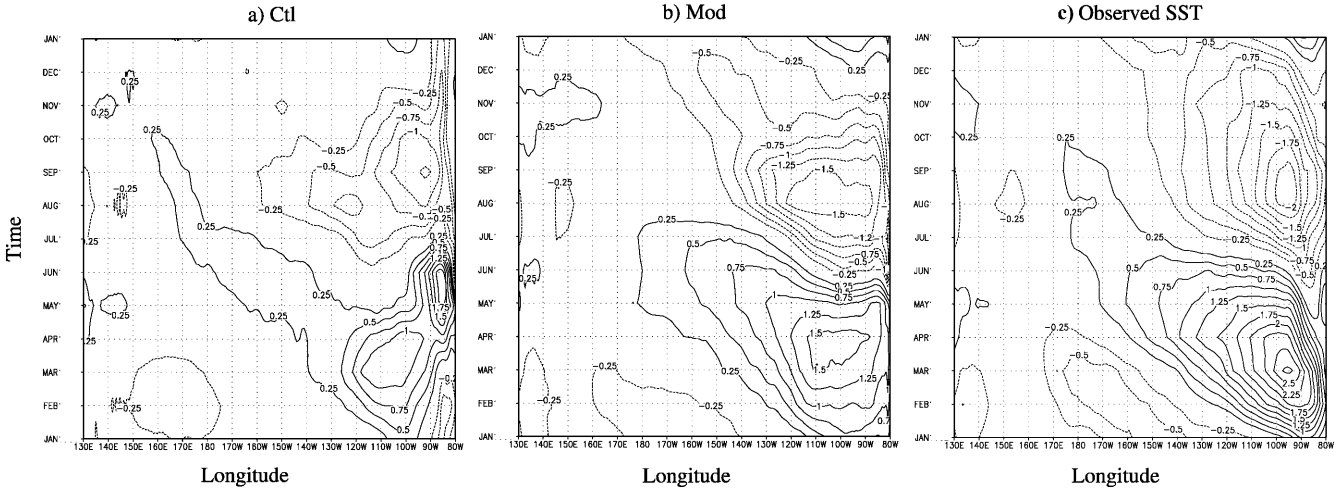

Fig. 3a–c Equatorial (2°S–2°N) SST seasonal cycle, with annual mean removed. **a** Reynolds observations, **b** Ctl1 run, **c** Ctl2 run

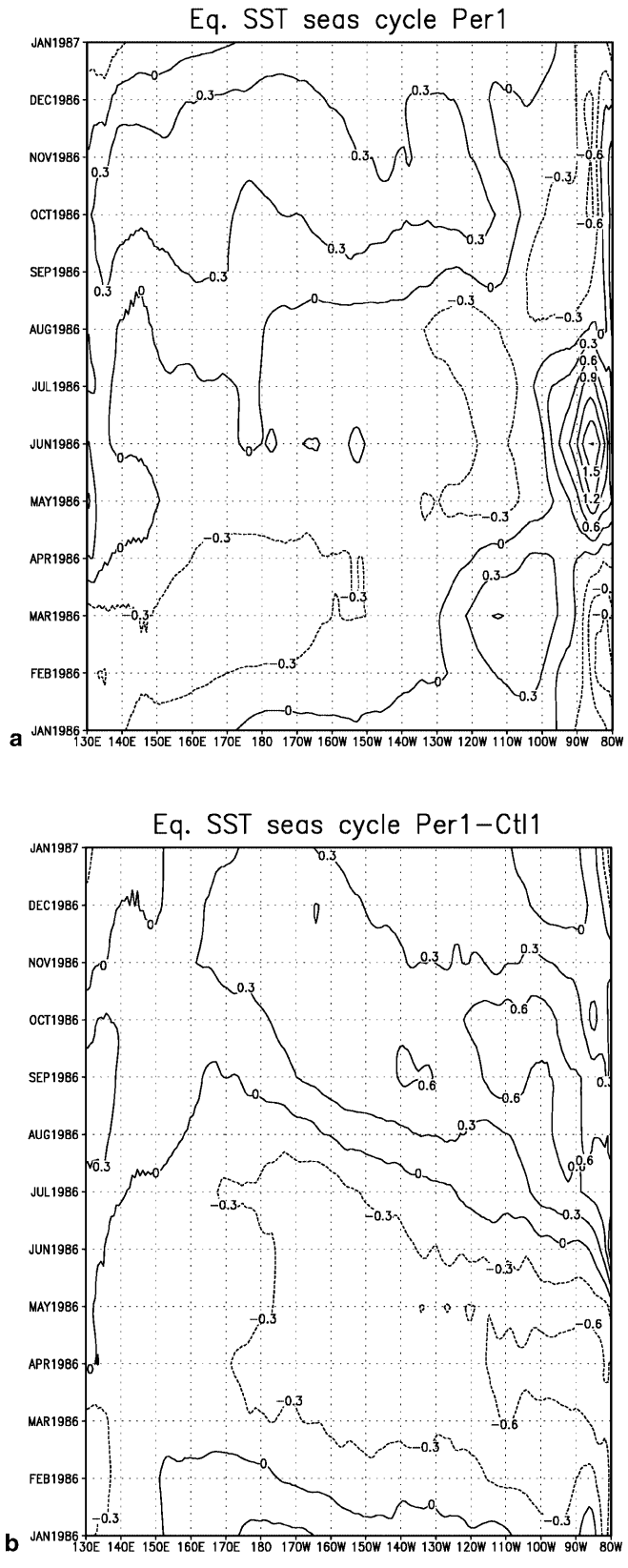

Fig. 4a, b Equatorial (2°S–2°N) SST seasonal cycle, annual-mean removed. **a** Perl simulation, **b** Perl-Ctl1 difference

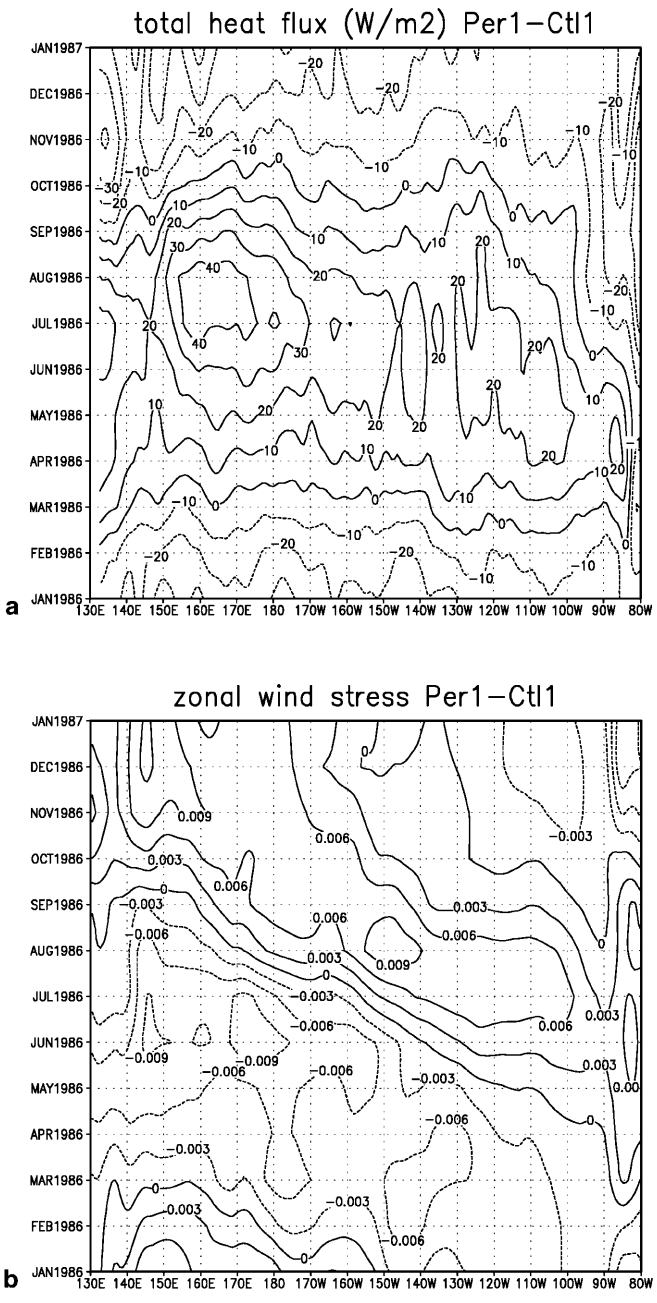

Fig. 5a, b Equatorial (2°S–2°N) seasonal Perl-Ctl1 differences. **a** Total surface heat flux in $W \cdot m^{-2}$, and **b** zonal wind stress in $N \cdot m^{-2}$

the central and western Pacific, thermocline temperature differences tend to oppose the surface ones, in the east the arrival of subsurface anomalies can explain the delayed response of SST to solar forcing. It is not clear if these thermocline depth changes in the east propagate from the west or are forced by local winds.

In the western Pacific, the temperature differences do not reach their maximum at the surface as in the east. This is consistent with for example in summer, the easterly wind stress cooling the mixed layer by stronger upwelling in depth, while the increased solar heat flux warms the surface.

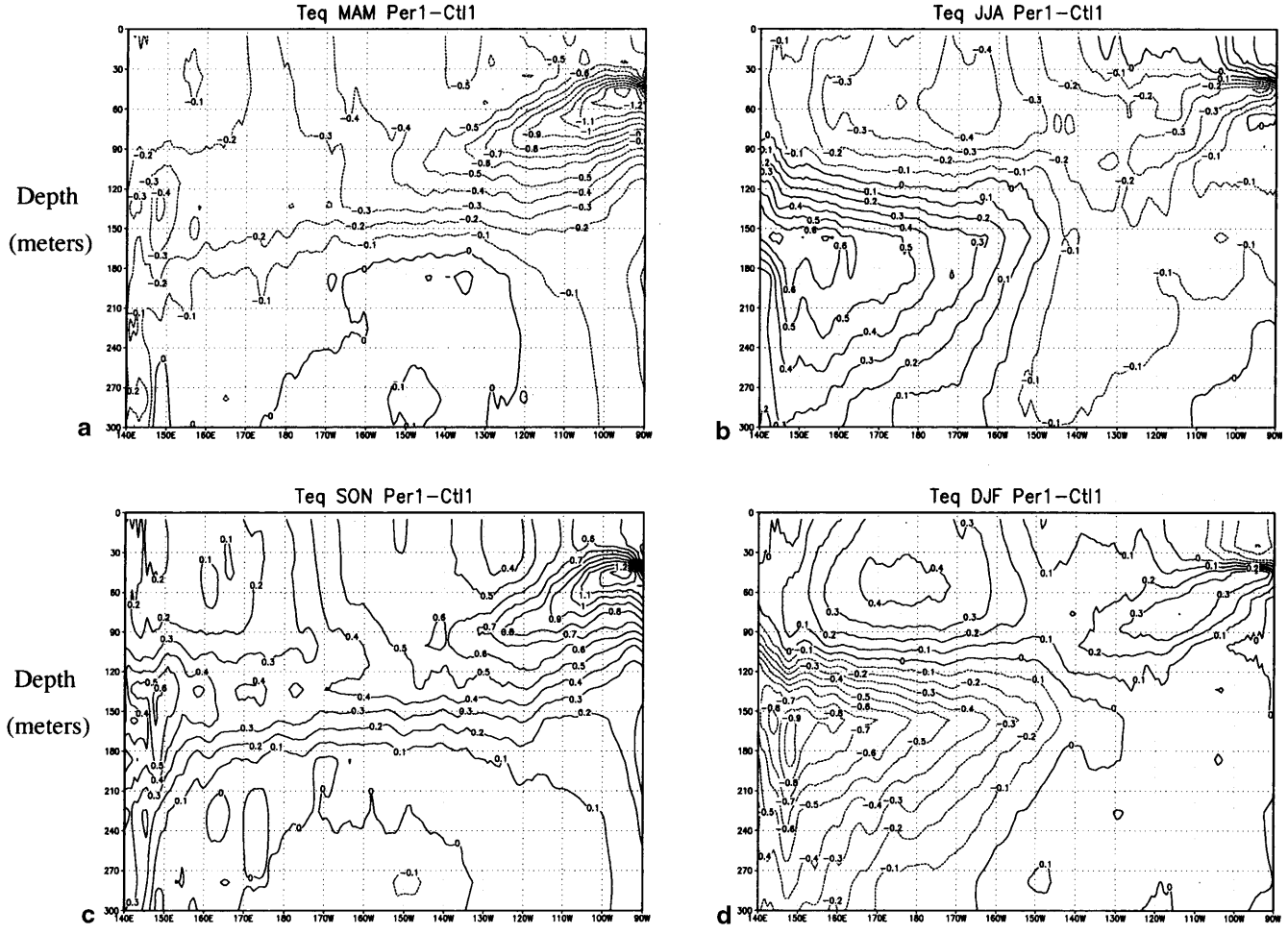

Fig. 6a–d Seasonal depth-longitude sections at the equator of the Perl-Ctl1 temperature differences. **a** MAM, **b** JJA, **c** SON, **d** DJF

To have a more quantified picture of the dominant effects in the Per1-Ctl1 temperature differences, we estimate the evolution of the mean mixed layer temperature T, as described in more details in the Appendix. The mixed layer depth is taken as the depth where the temperature is equal to SST −0.5 °C. The different terms contributing to the evolution of T are decomposed as follows:

$$\frac{\partial T}{\partial t} = Q_{sur} + Q_w + Q_T + Q_H$$

where Q_{sur} is the surface heat flux contribution, divided by the mixed layer depth, Q_H is the horizontal advection term, Q_w is the anomalous upwelling and entrainment of the mean temperature gradient, and Q_T is the mean vertical advection of anomalous temperature. The total advection, sum of Q_H, Q_w and Q_T, will be denoted Q_{adv}. The term by term difference of the evolution of T for the central Pacific (170°E–130°W) and western Pacific (140°E–160°E) region is given in Fig. 7. The $Q_{adv} + Q_{sur}$ total is shown together with $(\partial T/\partial t)$ to verify that their difference is weak.

In the central Pacific (Fig. 7a), the mixed layer temperature differences follow the surface fluxes closely. The different advection terms (Fig. 7b) tend to compensate each other, but none has an amplitude comparable to the surface flux. In the western Pacific (Fig. 7c) on the other hand, both Q_{adv} and Q_{sur} have a greater seasonal amplitude than the mixed layer temperature tendency, and balance each other. The detail of the advection term (Fig. 7d) show that it is dominated by Q_w confirming the strong influence of the upwelling induced by the zonal wind stress differences, which explains the weak surface temperature differences in the western Pacific.

3.2 Version 2 sensitivity

With the problems at the coast solved, the annual cycle of equatorial SST in the Ctl2 simulation has a greater amplitude than in Ctl1; the Per2 seasonal cycle (Fig. 8) is thus not as strongly modified as in the first version. The warm and cold periods in the east remain approximately the same, but the amplitude decreases. In the west, an

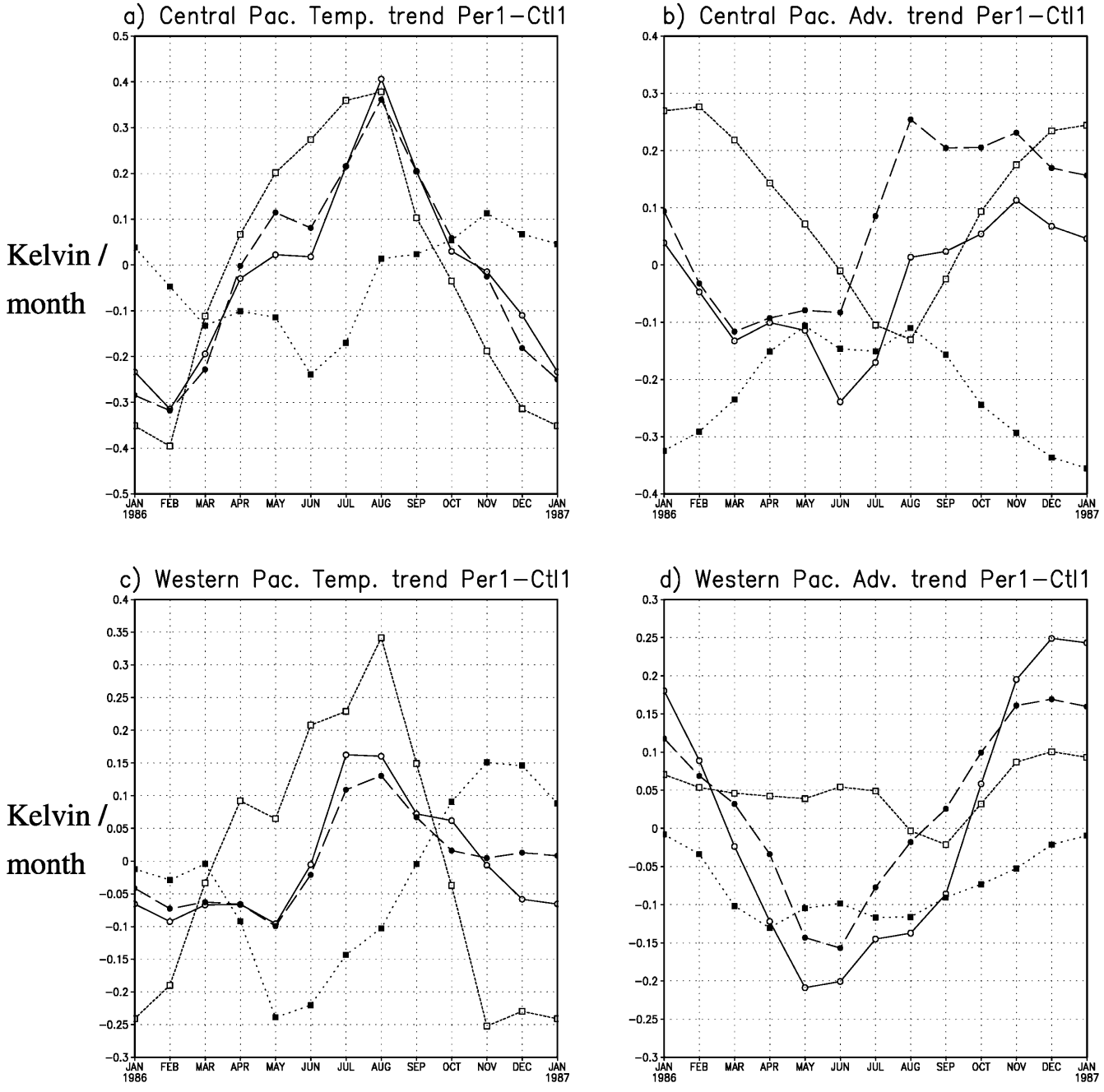

Fig. 7a–d Terms of the equatorial mixed layer temperature evolution: **a, b** Perl-Ctl1 differences in K · month^{-1}. **c, d** Central Pacific (170°E–130°W), Western Pacific (140°E–160°E). **a, c** $\partial T/\partial t$ *continuous line*, Q_{sur} *short dashes*, Q_{adv} *dots*, $Q_{adv} + Q_{sur}$ *long dashes*. **b, d** advection terms. Q_{adv} *continuous line*, Q_w *long dashes*, Q_T *short dashes*, Q_H *dots*

annual cycle develops, but does not extend as far east as in Per1. The amplitude of the SST differences between Per and Ctl is similar in the far western and eastern Pacific in the two versions, but there is no westward propagation in version 2. Instead, there is a hint of eastward propagation of surface anomalies from the west.

These changes between the two versions are reflected in the zonal wind stress differences (Fig. 9). In the eastern Pacific, wind stress anomalies are located to the west of anomalous SSTs, with an amplitude similar to version 1, but do not propagate. In the western Pacific, wind stress differences also follow roughly SST gradients, and thus propagate slowly eastward; but they have a much greater amplitude than in the eastern half of the basin.

The surface heat flux changes (Fig. 9) are not very different from version 1. The shortwave feedback term follows the underlying SST differences, and the heat flux seasonal cycle has its maximum amplitude in the central Pacific. This is however a region where both the SST and

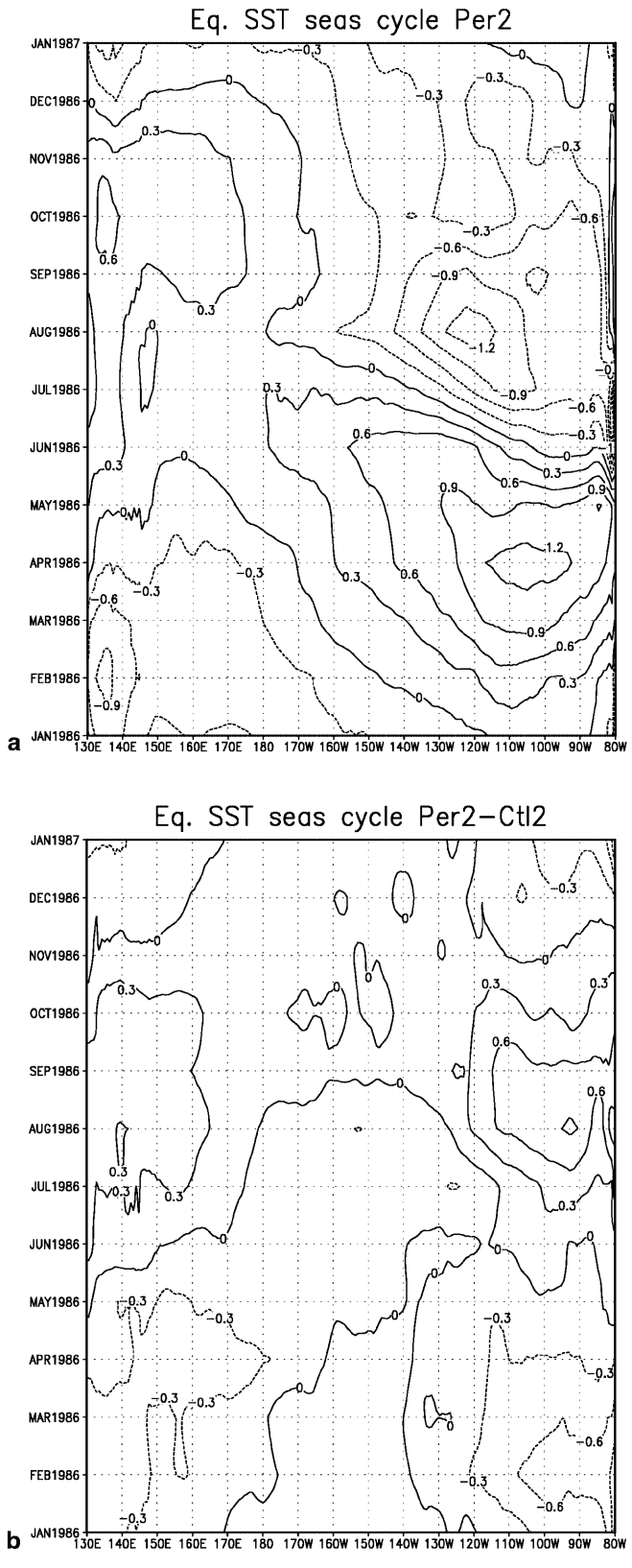

Fig. 8a, b Equatorial (2°S–2°N) SST seasonal cycle, annual-mean removed. **a** Per2 simulation, **b** Per2-Ctl2 differences

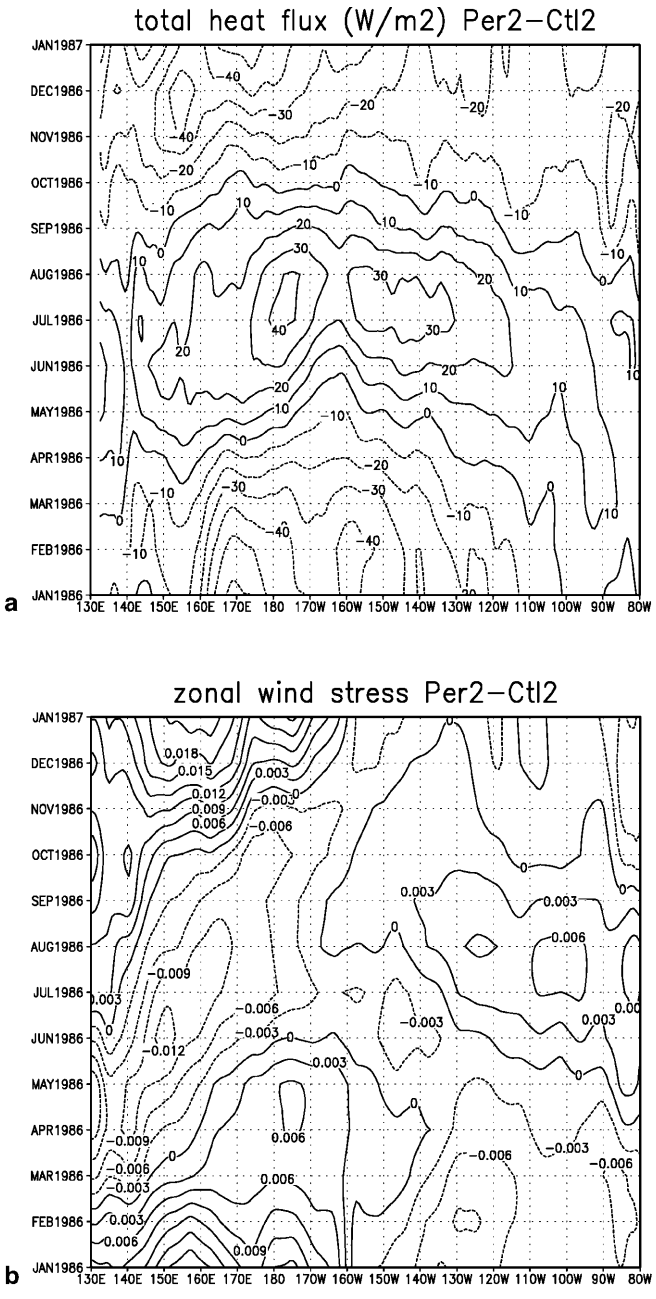

Fig. 9a, b Equatorial (2°S–2°N) seasonal Per2–Ctl2 differences. **a** Total surface heat flux in $W \cdot m^{-2}$; and **b** zonal wind stress in $N \cdot m^{-2}$

zonal wind stress differences between Per2 and Ctl2 are weak. The coupled mechanism identified for the first version thus cannot work here.

An explanation can be found in the subsurface temperature differences (Fig. 10). In summer and winter, large temperature differences centered at the thermocline depth are apparent in the central Pacific, and extend up to the surface. The upwelling of these anomalous temperatures would oppose the surface heat flux. These thermocline depth differences propagate from the west. Comparison with the wind stress differences shows that the thermocline zonal gradient is approximately in

balance with the wind stress, with warm (cold) anomalies to the east of westerly (easterly) stress. The eastward propagation is slower than Kelvin wave speed, it is closer to a coupled wind stress-thermocline-SST slow mode as described by Neelin (1991).

Examination of the terms of the mixed layer temperature evolution (Fig. 11) confirms the hypothesis: in the central Pacific region (Fig. 11a), the surface heat flux is in near balance with the advection term, the temperature tendency being only a residual term. Figure 11b shows that Q_{adv} is dominated as expected by the upwelling of anomalous temperature. The very large amplitude of Q_{sur} and Q_T comes in part from differences in the mixed layer depth caused by the subsurface temperature differences, which explain about one half of each term. In the western Pacific (Fig. 11c), the thermocline is too deep, and Q_T is small (Fig. 11d). The temperature evolution is thus dominated by the surface flux.

3.3 Discussion

The mechanisms of the coupled dynamical response to the shift of perihelion are thus very different in the two versions of the coupled model. Neelin (1991) identified two different coupled ocean-atmosphere feedbacks called slow SST modes: the atmospheric response to a warm SST anomaly consists in the zonal direction in westerlies to the west and above the anomaly, and easterlies to the east (Gill 1980). The anomalous westerlies decrease the upwelling, increase zonal and meridional heat advection in the cold tongue region, and decrease entrainment and evaporative cooling (in a mean easterlies background). All these effects considered together are designed as surface feedback, and lead to westward propagation of the SST anomaly. On the other hand, the anomalous wind stress forces a thermocline depth gradient. In the case of a warm anomaly, the deepest thermocline is to the east of the SST anomaly, thus contributing to its eastward propagation. This is called the thermocline feedback. It seems that version 1 sensitivity was dominated by a surface-type feedback, while the thermocline response is stronger in version 2. So what changes in the background state caused this change of behavior?

The mean easterly trade winds are stronger in the first version over the western and central Pacific (Fig. 2). As the turbulent entrainment cooling response to anomalous wind stress is non-linear, this can favor the surface feedback.

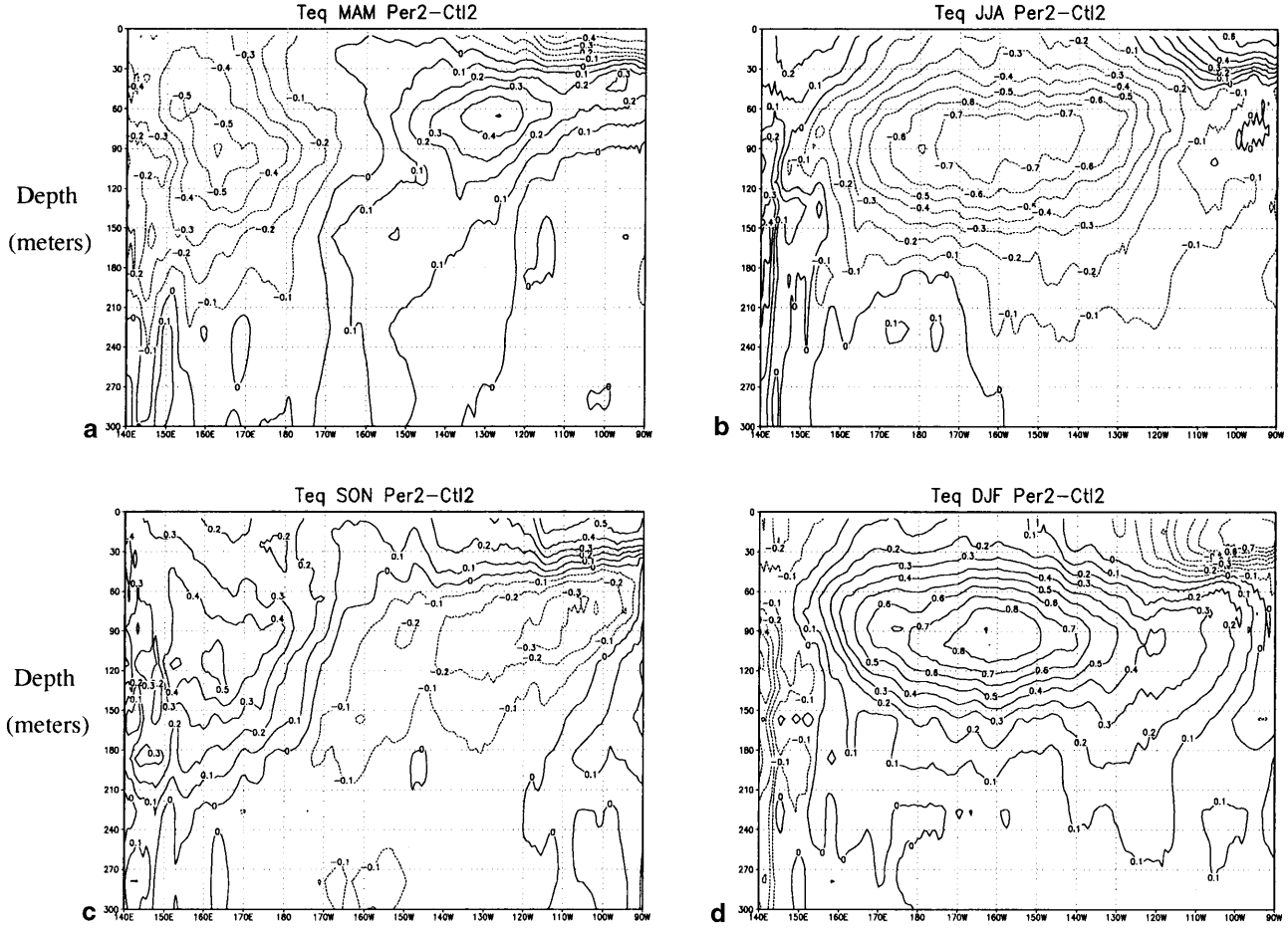

Fig. 10a–d Seasonal depth-longitude sections at the equator of the Per2-Ctl2 temperature differences. **a** MAM, **b** JJA, **c** SON, **d** DJF

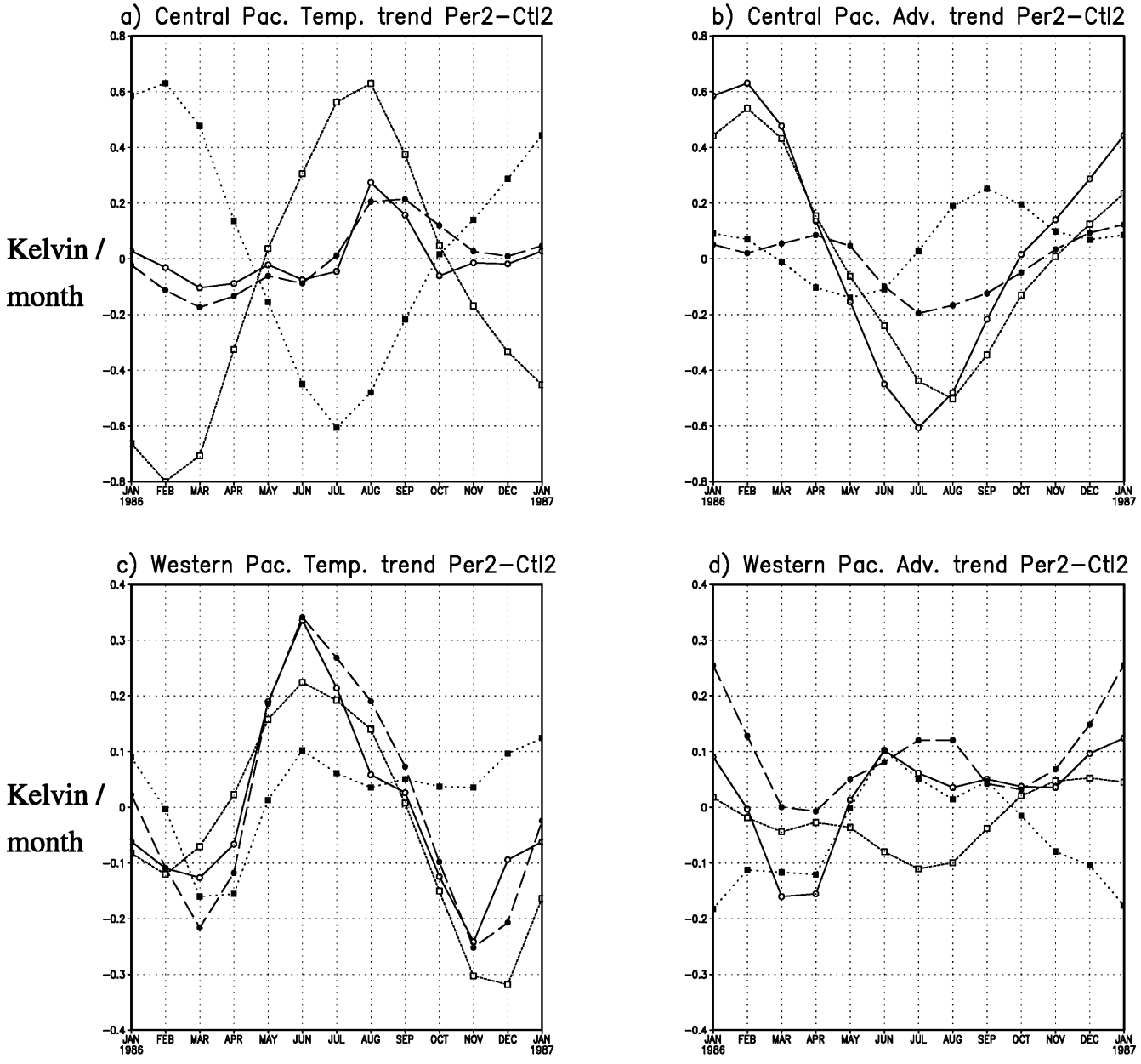

Fig. 11a–d Terms of the equatorial mixed layer temperature evolution: **a, b** Per2-Ctl2 differences in K · month^{-1}, **c, d** in Central Pacific (170°E–130°W); Western Pacific (140°E–160°E). **a, c** $\partial T/\partial t$ *continuous line*, Q_{sur} *short dash*, Q_{adv} *dots*, $Q_{adv} + Q_{sur}$ *long dash*. **b, d** advection terms. Q_{adv} *continuous line*, Q_w *long dash*, Q_T *short dash*, Q_H *dots*

The atmospheric response to SST anomalies is also different in the two versions. Figure 12 shows maps of the mean winter (DJF) differences in SST, precipitation and zonal wind stress between Per1 and Ctl1, and Per2 and Ctl2. The SST differences (Fig. 12a, d) have a similar pattern and amplitude in both experiments: the surface temperature is cooler in the Per run except in the central equatorial Pacific where it is slightly warmer. The precipitation response is however different: in both cases there is a rainfall increase to the west of the warmer SST patch, but it is stronger and extends further over to the southeast in version 2. The rainfall decrease over the southwest of the SPCZ and the eastern Pacific ITCZ is also much stronger. This must be a consequence of the larger warm pool in the version 2 control climate: over the warmer SSTs, the air column is more unstable, and the amount of available water vapor is greater, so the convective response to a SST anomaly is stronger than over the cooler area with increased subsidence of version 1 (Bony et al. 1997). In version 2, the stronger wind stress response in the western Pacific large-scale convergence area forces larger subsurface temperature differences in the central Pacific. The wind stress response to eastern Pacific SST differences on the other hand has the same amplitude, the eastward propagation is thus favored.

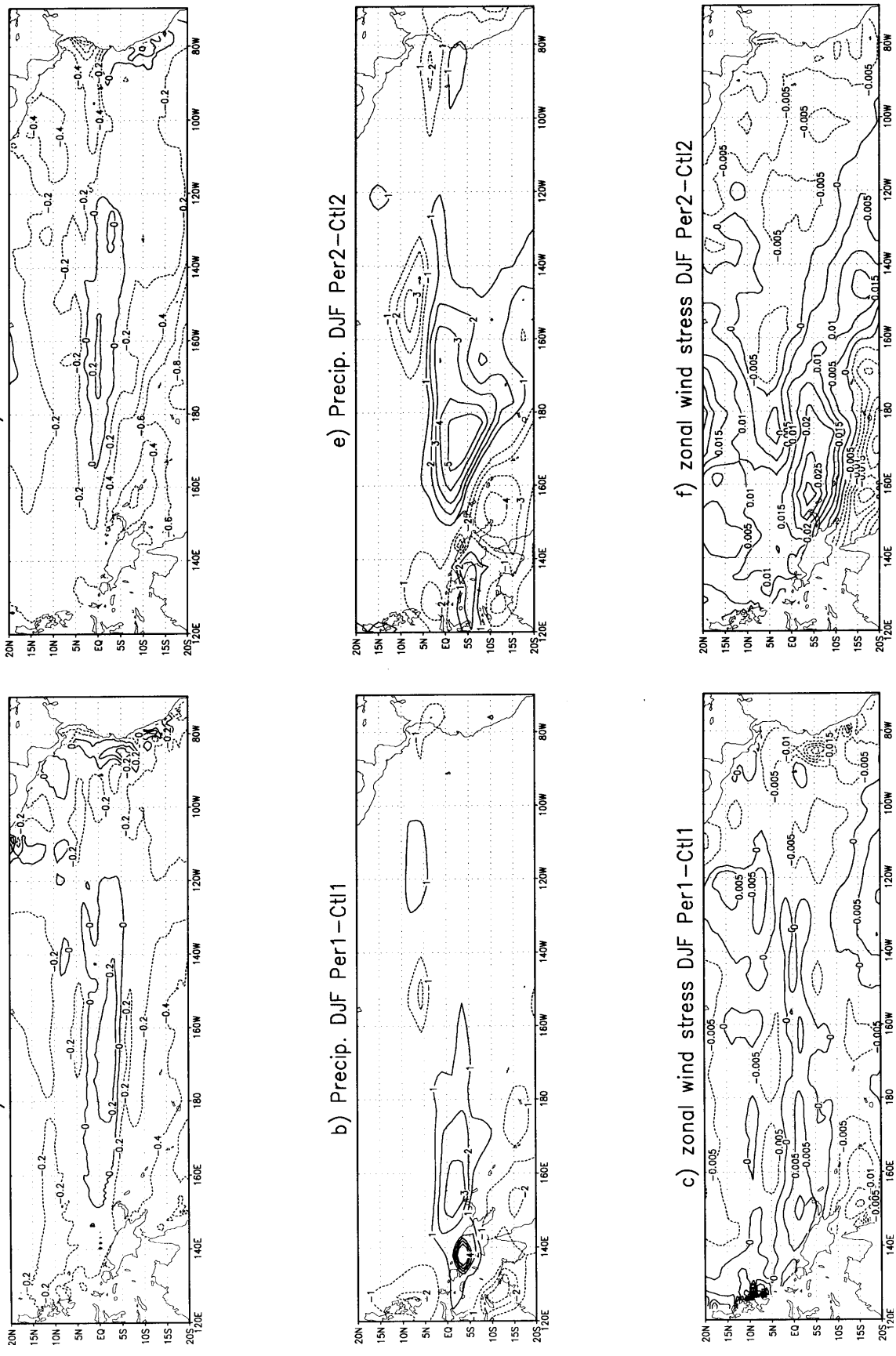

Fig. 12a–f Mean winter (DJF) differences between Per1-Ctl1 (*left*) and Per2-Ctl2 (*right*): **a, d** SST, **b, e** precipitation in mm · day^{-1}, and **c, f** zonal wind stress in N · m^{-2}

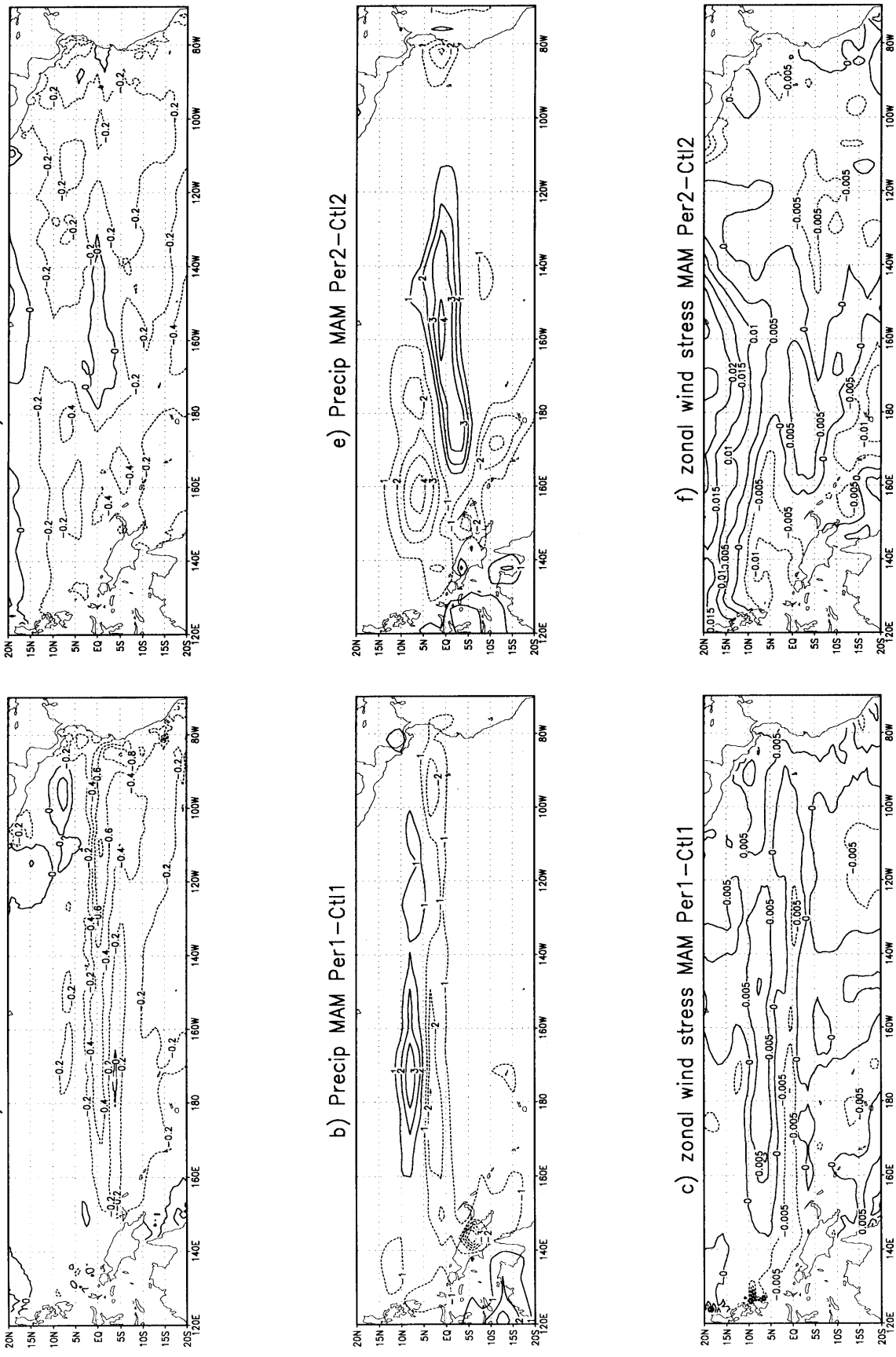

Fig. 13a–f Mean spring (MAM) differences between Per1-Ctl1 (*left*) and Per2-Ctl2 (*right*): **a, d** SST, **b, c** precipitation in mm · day^{-1}, and **c, f** zonal wind stress in N · m^{-2}

Another factor is the meridional structure of the atmospheric response. Figure 13 is the same as Fig. 12 but for spring (MAM). The SST differences are this time very different: in Per1-Ctl1, there is a strengthened cold tongue on the equator, and slightly cooler SST elsewhere. The precipitation response is weak (Fig. 13b), only a small poleward shift of the ITCZ. The wind stress differences are forced by the SST gradients, and have a very zonal structure: a thin band of easterlies on the equator and westerlies between 5–10°N. There is thus a strong off-equatorial negative wind stress curl response, which forces warm temperature differences at the thermocline depth: either by reflection of downwelling Rossby waves off the west coast, or by the increased subsurface meridional convergence (Vintzileos et al. 1999a). These warm temperatures are apparent during the next summer (Fig. 6).

In version 2, there is no SST difference in the central equatorial Pacific (Fig. 13d) because of subsurface warm anomalies, but elsewhere the SST is cooler in Per2, there are thus also zonal and meridional SST gradients. The precipitation map (Fig. 13e) shows a rainfall increase in the central Pacific, and two off-equatorial patches of decrease in the west. This structure is wider in the meridional direction than the underlying SST differences, and so is the wind stress difference (Fig. 13f). The wind stress curl is thus smaller than in Per1-Ctl1.

This stronger off-equatorial wind stress curl response in version 1 is confirmed by the comparison of the differences in the western Pacific zonal wind stress, and in the rate of change of the mean equatorial thermocline depth, which are well correlated both in Per1-Ctl1 and Per2-Ctl2, but with a twice as strong thermocline response in the former case (not shown). Thus, an equatorial westerly wind anomaly forced by warm SSTs in version 2 tends to force a deep thermocline to the east, while in the version 1 model, the thermocline tilt is the same, but the thermocline soon becomes shallower both to the east and west of the wind anomaly, preventing the eastward propagation of the SST anomaly.

4 Interannual variability

The simulated interannual variability is rather different in the two versions of the coupled GCM. In version 1, the ENSO signal is dominated by a quasi-biennal oscillation of weak amplitude (Vintzileos et al. 1999b). In version 2, both the period and amplitude have increased, and the modeled variability is much closer to the observed one (Codron et al. 2000b).

The change of the perihelion date was found to have little influence on the mean spatial structure and the mechanisms of ENSO in both versions. However, the differences in the mean seasonal cycle lead to a modification of the structure of ENSO time series. In the observations, the interannual anomalies tend to peak during the annual cold season in autumn (DeWitt and Schneider 1998). Figure 14 shows the values of the standard deviations of the Niño3 box anomalies for each month, together with the standard deviation of cold and warm anomalies only.

In version 1, the Niño3 anomalies have a weak seasonal cycle, with a standard deviation comprised between 0.35 and 0.5. Two small peaks correspond to the eastern Pacific cold phase in autumn, and to the influence of the spurious coastal upwelling in spring. The curves for warm and cold anomalies are very similar in the Ctl1 run, but in Per1 the cold anomalies tend to peak in spring, while warm anomalies are stronger in autumn.

The phase lock of ENSO on the seasonal cycle is stronger and more realistic in version 2: in the Ctl2 simulation, the variability is maximum in August, and much lower in spring. The standard deviation of warm anomalies is also higher than the one of cold anomalies for every month, indicating a tendency toward stronger and less frequent El Niño rather than La Niña events. This bias is reversed in the Per2 run: the variance of warm events remains low all year round, while the cold anomalies have a stronger variance in autumn and winter, and the same low variability as warm anomalies in March to July. The ENSO events also tend to peak later in the year, and the seasonal cycle of the variability is flatter than in Ctl2. The different occurrence of warm and cold events between Ctl2 and Per2 can also be observed by looking at the two Niño3 index time series (Fig. 15). In Ctl2, the climate is often in a weak cold state, with occasional strong and long El Niño events. The situation is symetric in Per2, although the Per2 cold events are shorter and more frequent than the Ctl2 warm events.

The appearance of warm or cold temperature anomalies at the surface in the eastern Pacific is mostly due to the upwelling of subsurface anomalies of the same sign due to thermocline movements. For a given deep temperature anomaly, the amplitude at the surface will be stronger when the upwelling is more efficient, or when the surface well-mixed layer depth is closer to the thermocline. This explains why the ENSO variance is greater in autumn, and weak in spring when the ocean surface is very stratified. In the Per2 simulation, the mixed layer depth has a smaller amplitude seasonal cycle than in Ctl2, and so does the interannual variability. A possible explanation for the different responses of warm and cold events may be that deep cold temperature anomalies due to thermocline displacement are centered above the mean thermocline position, while warm anomalies are deeper. The mean temperature of a shallow mixed layer may thus be influenced by a higher than average thermocline, but not by a deeper one. The mixed layer in Per2 is shallower than in Ctl2 in summer and autumn (Fig. 10). This may be enough to prevent the upwelling of warm anomalies, but not cold of ones. Similarly, the Per2 mixed layer is deeper in winter and spring, a season of mean weak vertical mixing. The Per2-Ctl2 difference may thus enhance selectively cold events variance,

because the mixed layer remains too shallow for strong El Niños.

5 Summary and conclusion

The sensitivity of the equatorial Pacific climate to a 6-month shift in the date of the perihelion was studied with two versions of a coupled GCM. The different parametrizations of the two atmospheric models have important direct effects on the modeled climate at the ocean boundaries. These effects result in a warmer mean SST at the equator in the second version, and an improved simulation of the eastern Pacific seasonal and interannual variability. The coupled response mechanism to the insolation change was also found to differ between the two versions.

In version 1, the eastern Pacific SST differences between Per1 and Ctl1 force a zonal wind stress response to the west. The resulting anomalous upwelling and vertical mixing then lead to a westward propagation of the initial SST differences. In the western Pacific, this propagating tendency opposes the local heat flux difference, and the SST sensitivity is small. This coupled feedback involves only the ocean surface layer. At the thermocline depth, the temperature differences forced by the strong off-equatorial wind stress curl are indeed of opposite sign to the SST differences.

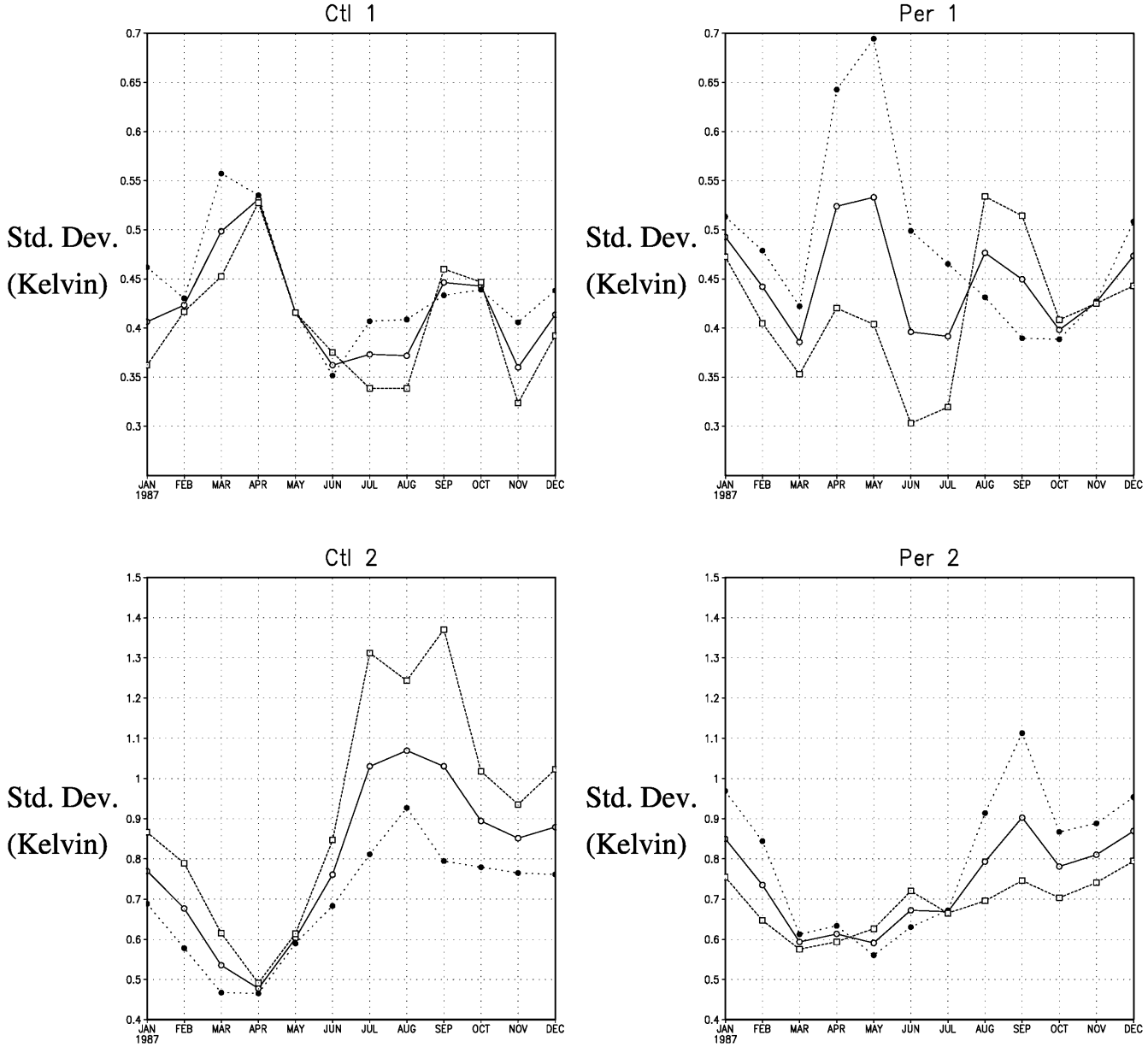

Fig. 14 Monthly standard deviation of Niño3 (150°W–90°W, 2°S–2°N) inter-annual anomalies for the four simulations. *Continuous line*: all anomalies, *dashed line*: warm events, *dotted line*: cold events. The scale is identical for Ctl1 and Per1 (*top*), and for Per2 and Ctl2 (*bottom*)

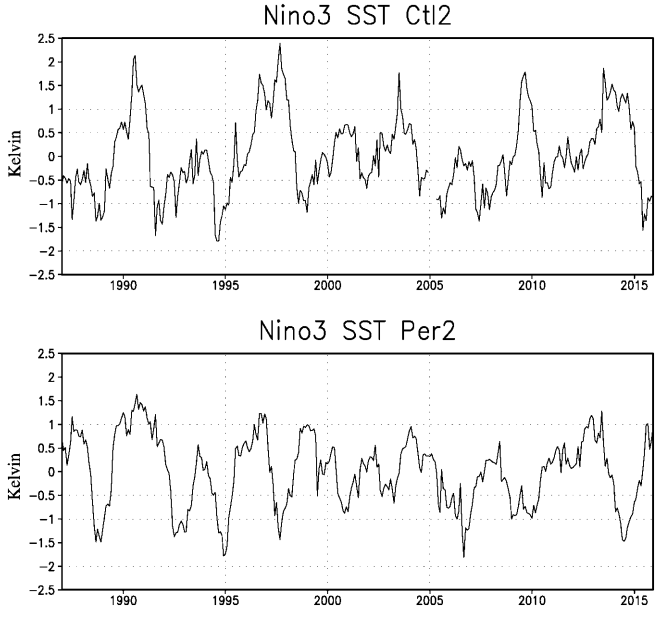

Fig. 15 Time series of the interannual Niño3 SST anomalies: Ctl2 run (*top*) and Per2 run (*bottom*). The first year has been suppressed

In version 2, the atmospheric convection sensitivity to SST differences is stronger in areas of the south and equatorial western Pacific where there is more mean large-scale convergence in Ctl2 than in Ctl1. The amplitude of the wind stress response to equatorial SST anomalies is consequently larger in the western Pacific than in the first model version, and its meridional structure is wider. This in turn forces a thermocline tilt under SST differences, but with fewer mean thermocline depth variations than in version 1. The subsurface temperature differences are thus of the same sign as the SST ones to the east, leading to a slow eastward propagation tendency. The weakest SST sensitivity amplitude is reached in the central Pacific in this version.

The two basic coupled mechanisms of surface and thermocline feedback identified as "slow SST modes" by Neelin (1991) thus coexist in the IPSL coupled GCM; and a mean SST change of about 1 °C in the equatorial cold tongue is sufficient to cause a shift from one dominant mode to the other in the response to the perihelion date shift. This result stresses the importance of a good representation of the observed climatology in the control simulation for sensitivity experiments.

The mean variance of interannual SST anomalies simulated for shifted perihelion conditions in version 2 does not change. As the eastern Pacific SST cycle has a lower amplitude in Per2 than in Ctl2, the phase-lock of ENSO with the seasonal cycle is weaker, and the events tend to peak later in the year, as found also by DeWitt and Schneider (1998). The most striking change is however a shift from a bias toward stronger El Niño rather than La Niña events in Ctl2 to a domination of cold events in Per2. That shift could be explained by a different sensitivity of warm and cold events evolution to a change in the mean mixed layer depth in the eastern Pacific.

The lack of very strong El Niño events in Per2 is consistent with paleoclimate data evidence (Sandweiss et al. 1996; McGlone et al. 1992; Rodbell et al. 1999); it shows that changes in orbital parameters can influence the tropical climate through their effect on ENSO variability. The relevance of this result to the early Holocene climate needs however to be confirmed by less idealized experiments including factors such as the obliquity changes and the global ocean response.

Appendix A: mixed layer temperature equation

To understand the evolution of SST in the different simulation, we study the energy balance of a well mixed surface layer.

The depth H of the mixed layer is computed for every month of each simulation as the depth at which the temperature becomes more than 0.5 °C cooler than the SST. Neglecting horizontal diffusion, the evolution of the mean temperature of the mixed layer $\bar{T}$ is:

$$\frac{\partial \bar{T}}{\partial t} = \frac{Q}{\rho C_p H} - \overrightarrow{\vec{U} \cdot \vec{\nabla}_H T} - \frac{w \cdot \Delta T}{H} \tag{1}$$

where

$$Q_{sur} = \frac{Q}{\rho C_p H} \tag{2}$$

is the surface heat flux contribution, after the solar radiation penetrating below the mixed layer has been substracted. The horizontal advection term averaged over the depth H is

$$Q_H = -\overrightarrow{\vec{U} \cdot \vec{\nabla}_H T} \tag{3}$$

The horizontal fluxes are computed every 5 days, to have a sufficient sample of the transient Legeckis (1977) waves contribution.

The vertical advection of heat through the bottom of the mixed layer is parametrized as: $-\left(\frac{w.\Delta T}{H}\right)$. ΔT represents the temperature jump at the base of the mixed layer. The upwelling velocity w is the sum of three terms:

$$w = w_{sub} + w_e + w_{ml} \tag{4}$$

where w_{sub} is the vertical velocity at depth H,

$$w_{ml} = \frac{\partial H}{\partial t} \tag{5}$$

is the contribution of mixed layer depth variations and is generally weak, and w_e is the turbulent entrainment velocity. The values of the vertical turbulent diffusion coefficient were not saved, so w_e is estimated by:

$$w_e = \frac{2mu_*^3}{\alpha g H \Delta T} \tag{6}$$

u_* being the surface friction velocity. Following Xie (1994), the coefficient m is taken as 2.5. The temperature jump ΔT value is estimated as close to 0.4 °C by fitting $w_{sub} \cdot \Delta T/H$ to $\frac{1}{H}\int_{-H}^{0} w \cdot T_z \, dz$, where T_z is the vertical temperature gradient. Both formulations yield similar results; the first one is used because it is easier to separate the dependence on w and H. Note that ΔT does not appear in the entrainment cooling contribution.

The terms on the right hand side of Eq. (1) are computed separately for the four simulations, and monthly means are formed.

When studying differences between two simulations a and b, the vertical advection term $w^a \cdot T_z^a - w^b \cdot T_z^b$ is further divided into two parts:

$$Q_w = 0.5 * (w^a - w^b) \cdot (T_z^a + T_z^b) \quad (7)$$

depends on the upwelling difference, and

$$Q_H = 0.5 * (w^a + w^b) \cdot (T_z^a - T_z^b) \quad (8)$$

is the contribution of different temperature profiles.

References

Andrich P, Delecluse P, Levy C, Madec G (1988) A multitasked general circulation model of the ocean. In: Science and engineering on Cray supercomputers. Proc Fourth Int Symp Cray Research Inc, pp 407–428

Bony S, Lau KM, Sud YC (1997) Sea surface temperature and large-scale circulation influences on tropical greenhouse effect and cloud radiative forcing. J Clim 10: 2055–2077

Bush ABG (1999) Assessing the impact of mid-Holocene insolation on the atmosphere ocean system. Geophy Res Lett 26(1): 99–102

Chang P (1993) Seasonal cycle of sea surface temperature and mixed layer heat budget in the tropical Pacific Ocean. Geophys. Res Lett 20: 2079–2082

Chang P (1996) The role of the dynamic ocean-atmosphere interaction in the tropical seasonal cycle. J Clim 9: 2973–2985

Chen D, Busalacchi AJ, Rothstein LM (1994) The roles of vertical mixing, solar radiation, and wind stress in a model simulation of the sea surface temperature seasonal cycle in the tropical Pacific Ocean. J Geophys Res C10: 20 345–20 359

Codron F, Vintzileos A, Sadourny R (2000a) An improved interpolation scheme between an atmospheric model and underlying surface grids near orography and ocean boundaries. Mon Weather Rev 128(4): 1177–1186

Codron F, Vintzileos A, Sadourny R (2000b) Influence of mean state changes on the structure of ENSO in a tropical coupled GCM. J Clim (in press)

de Noblet N, Braconnot P, Joussaume S, Masson V (1996) Sensitivity of simulated Asian and Africa summer monsoons to orbitally induced variations in insolation 126, 115 and 6 kBP. Clim Dyn 12: 589–603

DeVries TJ, Ortlieb L, Diaz A, Wells L, Hillaire-Marcel C (1997) Determining the early history of El Niño. Science 276: 965–966

DeWitt DG, Schneider EK (1998) The tropical ocean response to a change in orbital forcing. Tech. Rep 56, Center for Ocean-Land-Atmosphere Studies, July 1998

Fouquart Y, Bonnel B (1980) Computation of solar heating of the earth's atmosphere: a new parametrization. Beitr Phys Atmos 53(1): 35–62

Giese BS, Carton JA (1994) The seasonal cycle in a coupled ocean-atmosphere model. J Clim 7: 1208–1217

Gill AE (1980) Some simple solution for heat induced tropical circulations. Q J R Meteorol Soc 106: 447–462

Hall NMJ, Valdes PJ (1997) A GCM simulation of the climate 6000 years ago. J Clim 10: 3–17

Harzallah A, Sadourny R (1995) Internal versus SST-forced atmospheric variability as simulated by an atmospheric general circulation model. J Clim 8: 474–495

Hewitt CD, Mitchell JFB (1996) GCM simulations of the climate of 6 kyr BP: mean changes and interdecadal variability. J Clim 9: 3505–3529

Hewitt CD, Mitchell JFB (1998) A fully coupled GCM simulation of the climate of the mid-Holocene. Geophy Res Lett 25: 361–364

Koberle C, Philander SGH (1994) On the processes that control seasonal variations of sea surface temperatures in the tropical Pacific Ocean. Tellus 46A: 481–496

Kuo H (1965) On formation and intensification of tropical cyclones through latent heat release by cumulus convection. J Atmos Sci 22: 40–63

Kutzbach JE, Gallimore RG (1988) Sensitivity of a coupled atmosphere/mixed layer ocean model to changes in orbital forcing at 9000 years BPJ Geophys Res D1: 803–821

Le Treut H, Li Z-X (1991) Sensitivity of an atmospheric general circulation model to prescribed SST changes: feedback effects associated with the simulation of cloud optical properties. Clim Dyn 5: 175–187

Legeckis R (1977) Long waves in the eastern equatorial Pacific Ocean: a view from a geostationary satellite. Science 197: 1179–1181

Levitus S (1982) Climatological atlas of the world ocean. NOAA Prof Pap 13 US Government Printing Office, Washington, D.C., USA

Li T, Philander SGH (1996) On the annual cycle of the eastern equatorial Pacific. J Clim 9: 2986–2998

Manabe S, Strickler R (1964) Thermal equilibrium of the atmosphere with a convective adjustment. J Atmos Sci 21: 361–385

Masson V, Joussaume S (1997) Energetics of the 6000-yr BP atmospheric circulation in boreal summer, from large-scale to monsoon areas: a study with two versions of the LMD AGCM. J Clim 10: 2888–2903

McGlone MS, Kershaw AP, Markgraf V (1992) El Niño/Southern oscillation climatic variability in Australasian and South American paleoenvironmental records. In: Diaz HF, Markgraf V (eds) El Niño. Historical and paleoclimatic aspects of the southern oscillation. Cambridge University Press, New York, pp 435–462

Morcrette JJ (1991) Radiation and cloud radiative properties in the ECMWF operational weather forecast model. J Geophys Res 96: 9121–9132

Neelin JD (1991) The slow sea-surface temperature mode and the fast-wave limit: analytic theory for tropical interannual oscillations and experiments in a hybrid coupled model. J Atmos Sci 48: 584–606

Nigam S, Chao Y (1996) Evolution dynamics of tropical ocean-atmosphere annual cycle variability. J Clim 9: 3187–3205

Otto-Bliesner BL (1999) El Niño/La Niña and Sahel precipitation during the middle holocene. Geophy Res Lett 26(1): 87–90

Philander SGH, Gu D, Halpern D, Lambert G, Lau N.-C, Li T, Pacanowski RC (1996) Why the ITCZ is mostly north of the equator? J Clim 9: 2958–2972

Ramanathan V, Collins W (1991) Thermodynamic regulation of ocean warming by cirrus clouds deduced from observations of the 1987 El Niño. Nature 351: 27–32

Reynolds RW, Marsico DC (1993) An improved real-time global sea surface temperature analysis. J Clim 6: 114–119

Rodbell DT, Seltzer GO, Anderson DM, Abbot MB, Enfield DB, Newman JH (1999) An 15 000-year record of El Niño-driven alluviation in southwestern ecuador. Science 283: 516–520

Sadourny R (1975) The dynamics of finite-difference models of the shallow-water equations. J Atmos Sci 32: 680–689

Sandweiss DH, Richardson III JB, Reitz EJ, Rollins HB, Maasch KA (1996) Geoarchaeological evidence from peru for a 5000 years BP onset of El Niño. Science 273: 1531–1533

Schneider EK (1996) A note on the annual cycle of sea surface temperature at the equator. Tech Rep 36, COLA, Calverton, MD

Spencer RW (1993) Global oceanic precipitation from the MSU during 1979–1991 and comparison with other climatologies. J Clim 6: 1301–1326

Stricherz J, O'Brien JJ, Legler DM (1992) Atlas of Florida State University tropical Pacific winds for TOGA 1966–1985. Florida State University Tallahassee, pp 275

Stricherz J, Legler DM, O'Brien JJ (1997) TOGA pseudo-stress atlas 1985–1994, volume II: Pacific Ocean. Florida State University Tallahassee, pp 155

Vettoretti G, Peltier WR, McFarlane NA (1998) Simulations of mid-Holocene climate using an atmospheric general circulation model. J Clim 11: 2607–2627

Vintzileos A, Sadourny R (1997) A general interface between an atmospheric general circulation model and underlying ocean and land surface models: delocalized physics scheme. Mon Weather Rev 125(5): 926–941

Vintzileos A, Delecluse P, Sadourny R (1999a) On the mechanisms in a tropical ocean-global atmosphere general circulation model. Part I: mean state and the seasonal cycle. Clim Dyn 15: 43–62

Vintzileos A, Delecluse P, Sadourny R (1999b) On the mechanisms in a tropical ocean-global atmosphere general circulation model. Part II: interannual variability and its relation to the seasonal cycle. Clim Dyn 15: 63–80

Xie S-P (1994) On the genesis of the equatorial annual cycle. J Clim 7: 2008–2013